Acta Mech 227, 2025–2037 (2016)
DOI 10.1007/s00707-016-1612-7

ORIGINAL PAPER

Zhilong Peng · Cong Wang · Shaohua Chen

The microstructure morphology on ant footpads and its effect on ant adhesion

Received: 15 December 2015 / Revised: 22 February 2016 / Published online: 8 April 2016

Abstract Ants show a bionic application prospect due to their special climbing ability. However, different ant species living in different environments exhibit different adhesion abilities. In order to reveal their mechanical mechanisms, footpads of four representative ant species are investigated experimentally. Regular microstructures on the ventral side of ant footpads are clearly observed, which possess different shapes and sizes for different ant species. The normal adhesion force for each kind of ant is further measured with a spinning technique, which is significantly affected by the microstructure on the ventral surface of ant footpads. Theoretical models are established in order to disclose the mechanical mechanism, in which both the capillary force and the van der Waals interaction are considered. It is found that the real contact area depends significantly on the microstructures on the ventral side, which further affects the total adhesion force. The coexistence mechanism of wet and dry adhesion for ant footpads is proposed. The finding in the present paper should be useful for deep understanding of the adhesion mechanism of different ant species and helpful for the design of bio-inspired intelligent adhesion surfaces.

1 Introduction

Many animals and insects in nature have reversible adhesion abilities on various surfaces in their living environments. It is so interesting that different adhesion mechanisms have been studied experimentally and theoretically for decades. According to the morphology of the adhesion surface, the adhesion system has been categorized into hairy pads and smooth ones [1,2]. In the former, surfaces are covered with relatively long deformable setae with thin-film tips of different shapes [3–5]. For example, for geckos and lizards, as representatives of dry adhesion, van der Waals force is believed to be the leading actor [6]. For others, like beetles and flies, as representatives of wet adhesion, the capillary force dominates their adhesion [7]. In the latter, adhesion surface is covered with soft cuticle. Mysterious mucus secreted from glands provides adhesion force, e.g., tree frogs and bush crickets [8,9].

However, even on a smooth adhesion surface, highly specialized substructures were further observed. For example, the footpad of tree frogs is patterned with regular hexagonal microstructures of approximately 10-μm-diameter epidermal cells separated by approximately 1-μm-wide channels. Each surface cell is further covered with a similar but much finer microstructure of approximate 0.1- to 0.4-μm-diameter pegs [8]. The adhesion pad of bush crickets is also divided by similar hexagonal micro-units of approximately 14.7 μm^2 area [10]. The splitting mechanism of smooth adhesion surface has been thought of as a general design principle in many biological adhesion systems, which has been proved to significantly enhance the adhesion force not only for dry adhesion but also for capillary one [11–14].

Z. Peng · C. Wang · S. Chen (✉)
LNM, Institute of Mechanics, Chinese Academy of Sciences, Beijing 100190, China
E-mail: chenshaohua72@hotmail.com
Tel.: 86-10-82543960
Fax: 86-10-82543977

Ants, as typical bio-mimetic insects, have also received much attention. The final conclusion on ant footpads is that each footpad consists of a pair of claws and an arolium located between them [15,16]. On rough surfaces, the claw is used, while on smooth surfaces, the arolium that looks like a soft and foldable cuticular sac filled with fluid works. A mysterious mucus can be secreted from the arolium when an ant attaches to a smooth surface, which results in adhesion through capillary force. Do all ant species have the same adhesion ability? The answer is negative. The adhesion ability varies significantly between different ant species living in different environments. Federle et al. [17] found that arboreal ants have much better adhesion ability than those living on the ground, and different ants show significantly different adaptability to some specific surfaces. For example, only a few ant species are able to move on stems covered with epicuticular wax crystals. However, on smooth Perspex, the superior 'wax-runners' perform significantly worse than closely related congeners that are unable to climb on waxy stems [18]. What is the reason? All these indicate that not only the capillary force but also the van der Waals force may be adopted by ants. Both the adhesion energy and the wettability of different surfaces should influence the climbing ability of ants. Furthermore, is there any microstructure on the ventral surface of ant arolium, similar to the substructures on tree frog pads? If it is true, how does the microstructure on ant footpads affect their adhesion? All these are still open questions till now.

In this paper, we choose four representative ant species living in different environments to answer the above questions. Not only the contact area of adhesion footpads but also the ventral surface of the arolium is observed experimentally. The normal adhesion force of each kind of ants is measured, too. A simple theoretical model considering the morphology of microstructures on the arolium is further established, in which not only the capillary force but also the van der Waals interaction is involved. Both the theoretical analysis and experimental measurement suggest that a coexistence mechanism of wet and dry adhesion may be achieved by ants and the adhesion ability should be affected by the microstructures on ant footpads.

2 Experiment methodology

2.1 Specimen and experimental observation

Four kinds of ants are chosen in the present study. Arboreal ants, such as *Oecophylla smaragdina* and *Polyrhachis dives*, can run on most surfaces. *Camponotus japonicus* and *Diacamma rugosum* live on the ground and walk only slowly on an inclined smooth glass. The selected species possess similar sizes and approximate 5–10 mg in weights. All colonies are collected in south China and kept in laboratory nests, fed with honey water, fruits and dead insects.

Unlike the adhesion pad of grasshoppers or some other insects, the arolium of Hymenoptera is a foldable and soft cuticular sac, which is inflated in order to provide a contact surface when clinging on a substrate. In order to observe the ventral surface of an unfolded arolium on ant footpads, the experimental setup is shown in Fig. 1, where ants adhere upside down on a transparent glass. The real contact interface between the ventral surface of the unfolded arolium and the glass is observed with an optical microscope (Olympus BX51) equipped with reflected illumination. Images are captured with a CCD camera (COOLSNAP COLOR 3.3M).

After observing the microscopic image, we freeze the ant with liquid nitrogen (−190 °C) when it is adhering on a glass slip. Then, we can obtain an unfolded arolium, which helps us to observe the microstructure on its ventral surface. We cut off one ant leg at an environmental temperature of −100 °C and coat it with gold in vacuum. After this, the microstructure on the ventral surface of an unfolded arolium can be directly observed with SIRION400NC field emission microscopy (FEI, Netherlands).

2.2 Force measurement

Similar to Federle et al. [18], we adopt a centrifuge technique to measure the normal adhesion force of ants with a homemade instrument as shown in Fig. 2a. A schematic of the operating principle of the experimental setup is shown in Fig. 2b. The tested ants are placed on the lateral surface of the vertically smooth Plexiglas plate (PMMA) with a size of 12 cm × 15 cm as shown in Fig. 2b. It is driven by a rotor of radius 127 mm. The rotational velocity can be gradually accelerated from 0 to 2000 revs/min. The current velocity is measured by detecting the colored stripes on the rotor axis with a laser sensor, which is displayed on a digital panel attached outside the centrifuge. The whole procedure is also recorded by a digital camera. At a relative low rotating speed, the tested ant can run around on the plate. It will reach a 'freezing' state when the velocity of the centrifuge surpasses a threshold [15].

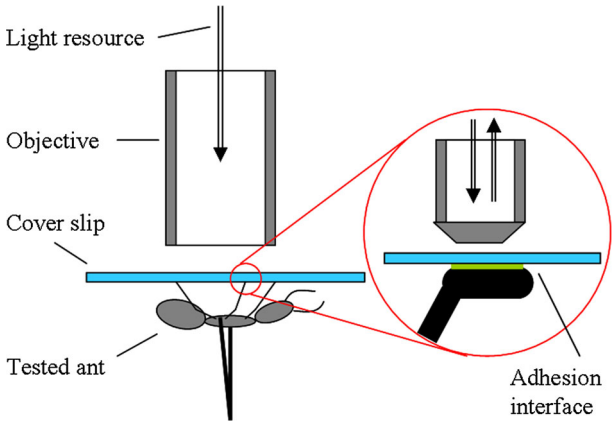

Fig. 1 Schematic of the experiment setup in order to observe the ventral surface of ant footpads in situ with an optical microscope, where the investigated ant is upside down on a transparent glass sheet

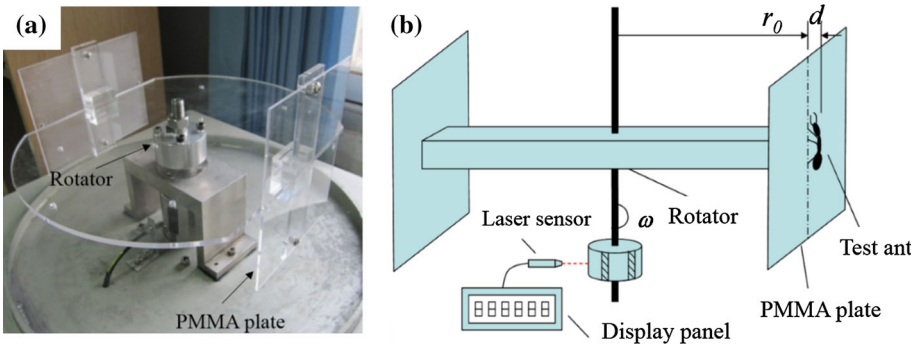

Fig. 2 Experiment setup in order to measure the normal adhesion force of a living ant. **a** The photograph of the experiment setup, which adopts the centrifugal technique; **b** schematic of the operating principle for measuring the normal adhesion force of a living ant, where ω is the angular velocity

The normal adhesion force of ants can be calculated as

$$F = m\,(r_0 + d)\,\omega^2, \tag{1}$$

where r_0 is the distance between the central axis and the PMMA plate as shown in Fig. 2b; m is the body mass of the tested ant and ω is the rotational speed at the moment of detachment. d is the distance between the mass center of the tested ant and the plate surface, which is about 2 mm.

Five active ants are selected for each species. The normal adhesion force is measured three times for each ant. The time interval is at least 15 min in order to ensure enough time for the ant to have a rest.

3 Experimental results

3.1 Morphology and microstructure of ant footpads

Comparison between the experimental observation [16] and that in the present one exhibits the same adhesive organ with a soft arolium locating between two claws at the end of a tarsus for different ant species. However, an interesting finding is that the ventral surface of ant arolia is not perfectly smooth but covered with finer regular patterns. The microstructure is obviously different among different ant species as shown in Fig. 3. Finely arranged hexagonal islands cover on the arolium surface of *O. smaragdina*, where each island with an area of about $26 \pm 6\,\mu m^2$ is separated by approximate 0.2-μm-wide channels as shown in Fig. 3a. The arolium surface of *P. dives* is divided into many separated conical-like microstructures as shown in Fig. 3b with an approximate area $2.8 \pm 0.9\,\mu m^2$ for each microstructure. A hair of about 0.2 μm diameter and 1 μm length

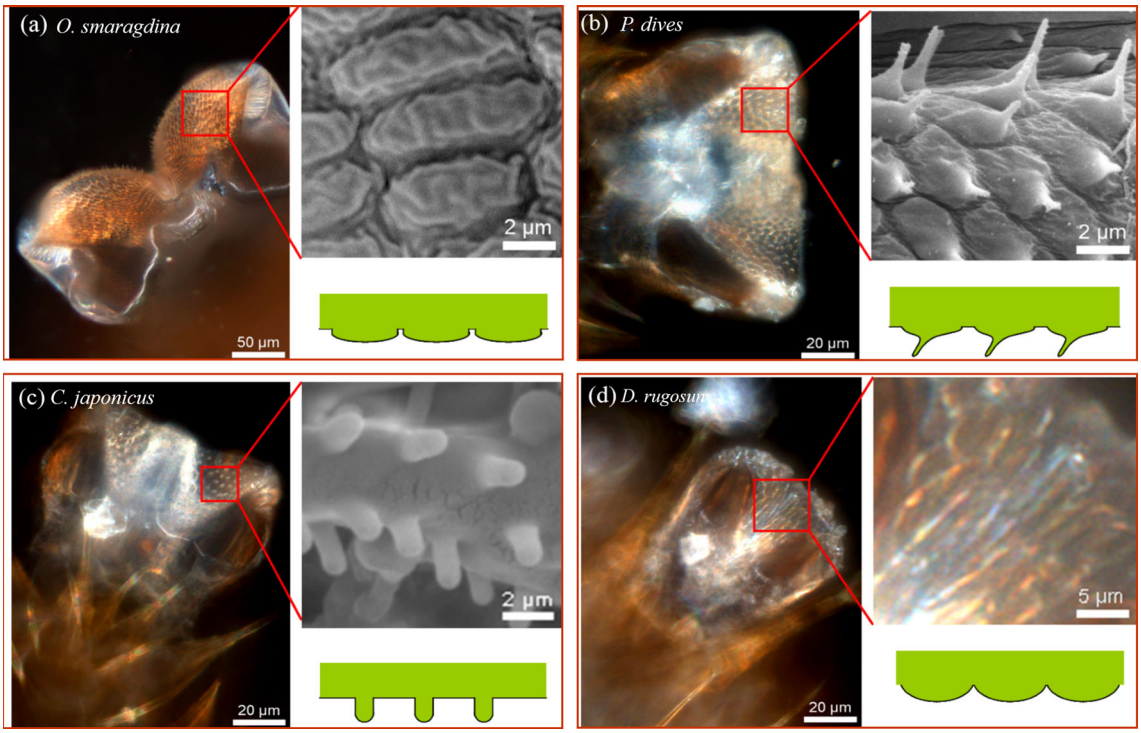

Fig. 3 Morphologies of microstructure on the ventral side of different ant footpads. **a** *O. smaragdina*; **b** *P. dives*; **c** *C. japonicus*; **d** *D. rugosum*

is observed on each microstructure also. On the cuticle of *C. japonicus* pads, no texture but separated tiny pillars are found, and each pillar is about 2μm tall with a diameter about $1\,\mu$m and an interval about $5\,\mu$m on average as shown in Fig. 3c. The arolium surfaces of *D. rugosum* are covered with closely and randomly arranged wrinkle-like strips, each of which has an area about $18 \pm 3\,\mu\text{m}^2$ and is divided by channels arranged in the same direction.

The microstructure on the ventral surface of footpads contacts directly the natural substrate, which should play a significant role in the adhesion behavior of the ant. Among the four kinds of ant species, the coverage ratio of the microstructures on *O. smaragdina* footpads is the largest since almost all the surface of the *O. smaragdina* arolium is covered with microstructures. The unfolded arolium of all four kinds of ants is symmetric with respect to its central axis, so that the contact area on a glass substrate looks like a B-shaped region under the optical microscope as shown in Fig. 4. It is consistent well with the observation in Federle et al. [19]. The contact area is further measured, and the average contact area is about $24{,}900\,\mu\text{m}^2$ for *O. smaragdina*, $4300\,\mu\text{m}^2$ for *P. dives*, $3500\,\mu\text{m}^2$ for *C. japonicus* and $2200\,\mu\text{m}^2$ for *D. rugosum*.

3.2 Adhesion force and adhesion strength of ant footpads

The adhesion force for each kind of ant on a smooth PMMA surface is measured using a centrifuge technique. It is found that arboreal ants generally have better adhesion ability than those living on the ground as shown in Fig. 5a. In particular, *O. smaragdina* shows an outstanding performance on smooth surfaces, whose adhesion force is about 70 times of their body weights.

The adhesion strength that is defined as the adhesion force per unit contact area is shown in Fig. 5b for the four kinds of ants. The hexagonal microstructure of *O. smaragdina* is the most efficient surface for adhesion, while the adhesion strength of *C. japonicus* with micro-pillars is only half of that of *O. smaragdina*. An in-between adhesive strength is owned by *P. dives*, which has both hexagonal structures and micro-hairs with high aspect ratio. Despite the weak adhesion force, *D. rugosum* has an adhesion strength almost similar to *P. dives*.

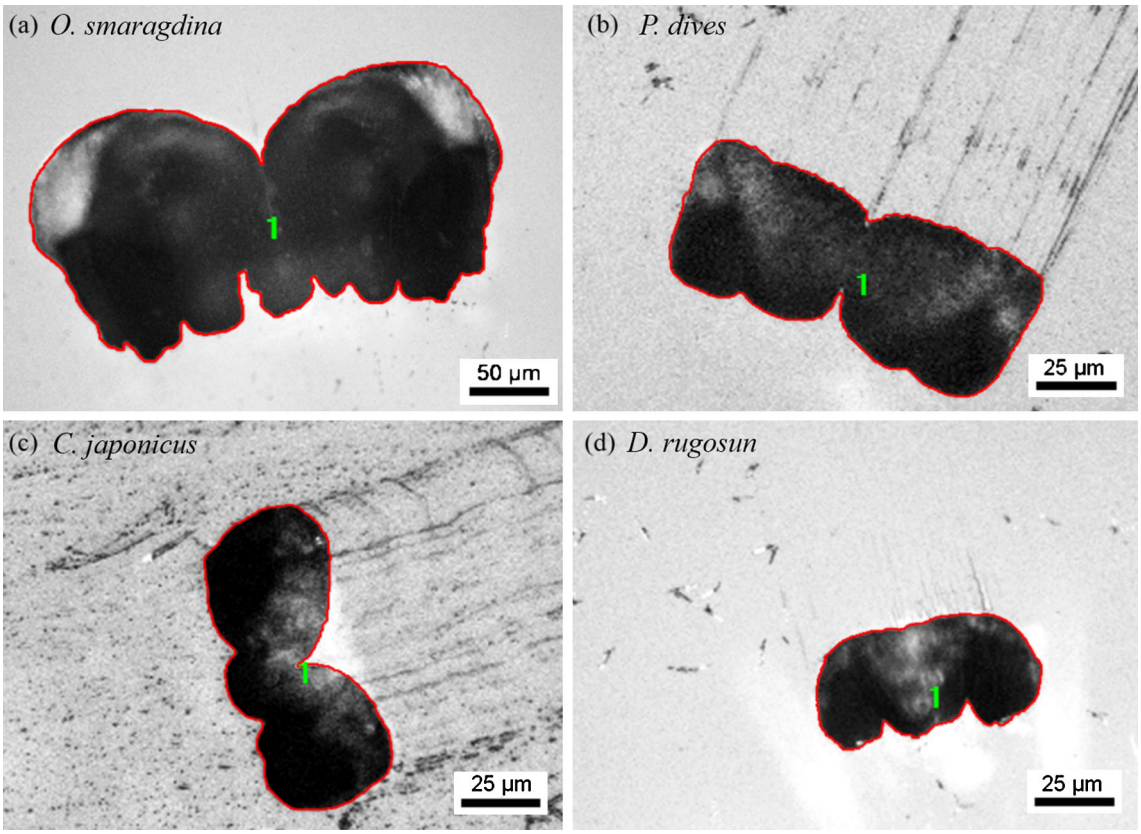

Fig. 4 Images of contact area of different ant aroliumlia, which is observed under a reflected illumination microscope. **a** *O. smaragdina*; **b** *P. dives*; **c** *C. japonicus*; *d D. rugosum*

4 Theoretical model

In order to understand the above mechanical mechanism, a generally theoretical model is established based on the experimental observation as shown in Fig. 6, in which a truncated conical indenter with a spherical tip contacts a flat substrate. Not only the adhesion of a single asperity but also the splitting effect is considered. Both the van der Waals interaction and the capillary one are included in the present analysis.

In this model, R is the radius of the cross section on the top of the cone, R_s is the radius of the sphere, α is half of the cone angle, θ_1 and θ_2 are contact angles between the liquid and the solid surfaces, respectively. D is the separation between the spherical tip and the substrate. ϕ is the filling angle. Parameters of the microstructure on the arolium for the four kinds of ant species are approximately taken as: (i) $\alpha = 0$ and $R_s \to \infty$ for the flat island of *O. smaragdina*; (ii) $\alpha = \pi/3$ and $R_s/R = 2$ for the conical asperity of *P. dives*; (iii) $\alpha = 0$ and $R_s/R = 1$ for the pillar of *C. japonicus*; (iv) $\alpha = 0$ and $R_s/R = 5$ for the stripe island of *D. rugosum*. The effect of liquid gravity is assumed to be negligible as well as the deformation of both the conical indenter and substrate.

4.1 The capillary force

We first consider the effect of microstructure on the capillary force. The capillary force consists of two parts [20]. One is due to the surface tension at the contact line and the other is induced by the pressure difference inside and outside the meniscus. The total capillary force can be written as [20–22]

$$F_c = -\pi b^2 \cdot \Delta p + 2\pi \gamma b \cos\theta, \tag{2}$$

where θ is the angle between the axial direction and the tangential direction of the surface tension (positive when anticlockwise) and b is the wetted radius on the tip as shown in Fig. 6. For convenience, the meniscus of

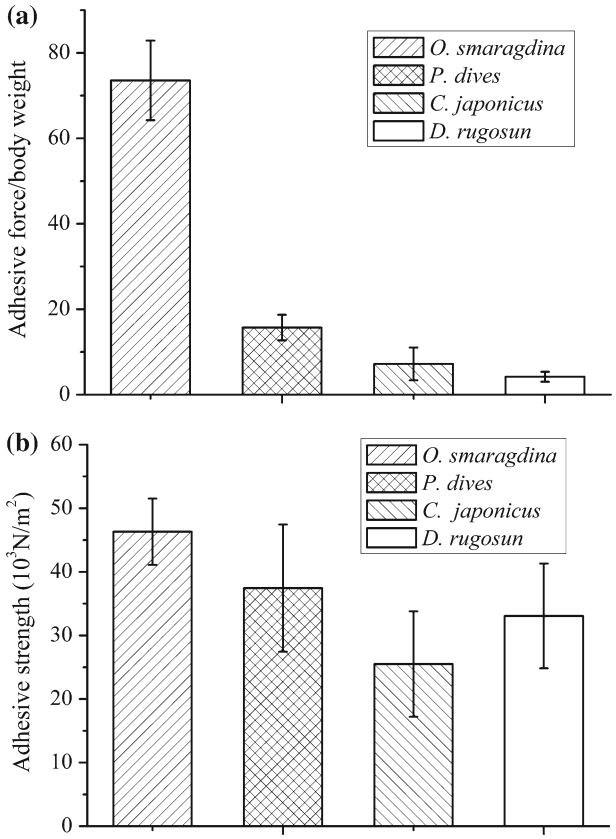

Fig. 5 The adhesion behavior of different ant species measured experimentally. **a** For the adhesion force; **b** for the adhesion strength

the liquid bridge is assumed to be a circular arc [20]. Then, the pressure difference is described by the Laplace equation as

$$\Delta p = \gamma \left(\frac{1}{l} - \frac{1}{r} \right), \tag{3}$$

where r and l are the two principal radii of curvatures.

The wetting configuration can be distinguished as three kinds of cases according to the liquid volume and the separation distance D between the truncated conical tip and substrate as shown in Fig. 6a–c.

(a) If the volume of liquid is relatively small, only a part of the truncated conical tip is wetted as shown in Fig. 6a. Then, we have $b < R$, $\theta = \pi/2 - \theta_1 - \phi$ and

$$\phi = \arcsin \frac{b}{R_s}. \tag{4}$$

The two principal radii of curvatures are

$$r = \frac{R_s \left(1 - \cos \phi\right) + D}{\cos \theta_2 + \sin \theta}, \tag{5}$$

$$l = b + r \left(\cos \theta - 1\right). \tag{6}$$

The volume of the liquid bridge V is

$$V = \int_0^{h_0} \pi G^2 \left(z\right) \cdot \mathrm{d}z - V_s, \tag{7}$$

where

$$G \left(x\right) = r + l - \sqrt{r^2 - \left(r \cos \theta_2 - z\right)^2}, \tag{8}$$

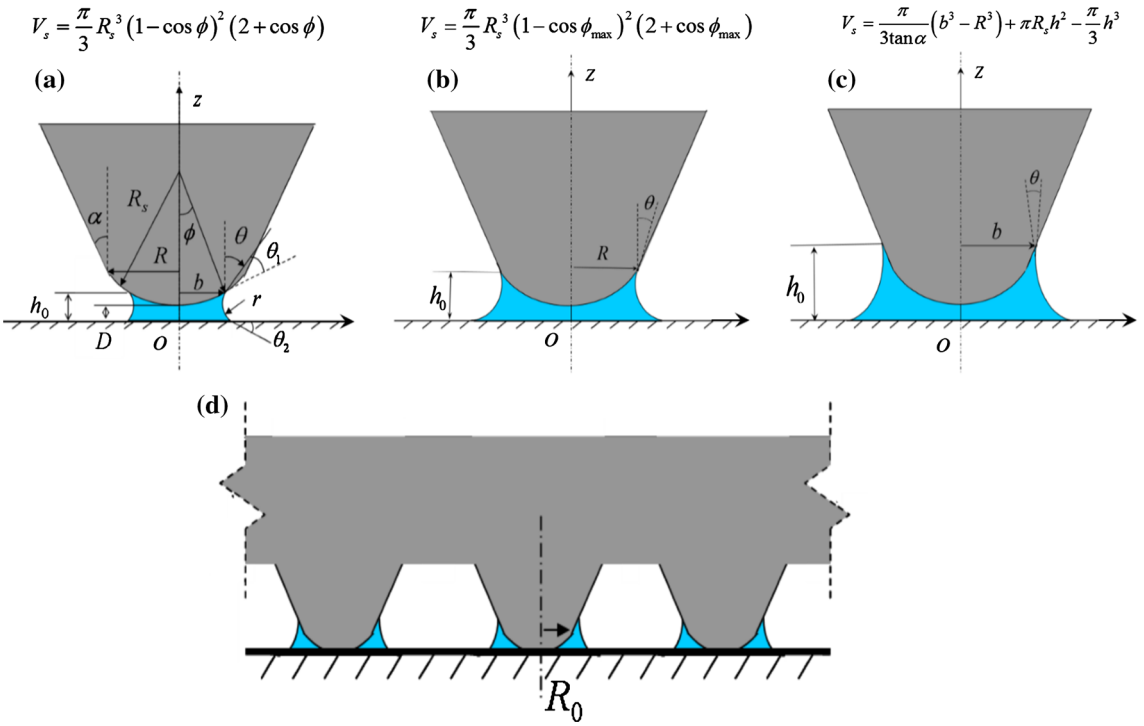

Fig. 6 Theoretical models of a truncated conical indenter with a spherical tip in wet adhesion on a smooth substrate. **a** Liquid only wets the spherical tip; **b** the liquid bridge is pinned at the joint of the spherical tip and the conical part; **c** liquid wets the conical surface; **d** a splitting model with self-similarity scaling to simulate multiple microstructures on ant footpads

and the immersed volume V_s is

$$V_s = \frac{\pi}{3} R_s^3 \left(1 - \cos\phi\right)^2 \left(2 + \cos\phi\right). \tag{9}$$

(b) In the intermediate wetting configuration as shown in Fig. 6b, the contact line is precisely pinned at the joint between the conical part and the spherical tip. Then, we have $b = R$ and $\phi = \phi_{\max} = \arcsin(R/R_s)$. The angle θ varies from $\pi/2 - \theta_1 - \phi_{\max}$ to $\alpha - \theta_1$. Equations (5)–(9) are still valid for this case. However, instead of the immersed radius b, the angle θ is a variable in this case.

(c) If the volume of liquid is relatively large, the contact line climbs on the conical part as shown in Fig. 6c. Then, we have $b > R$ and $\theta = \alpha - \theta_1$. The principal radius of curvature r is

$$r = \frac{\frac{b-R}{\tan\alpha} + h + D}{\cos\theta_2 + \sin\theta}, \tag{10}$$

where h is the height of the spherical cap,

$$h = R_s - \sqrt{R_s^2 - R^2}. \tag{11}$$

The volume of liquid bridge V can also be calculated by Eqs. (7) and (8) with an immersed volume

$$V_s = \frac{\pi}{3\tan\alpha}\left(b^3 - R^3\right) + \pi R_s h^2 - \frac{\pi}{3} h^3. \tag{12}$$

4.2 The van der Waals force

The capillary force cannot resist tangential sliding if viscous and dynamic effects are not considered. However, it is demonstrated experimentally that the friction force of ants is even larger than the normal adhesion force [19]. It is reasonable to assume that dry contact between ant footpads and substrates may occur. Therefore, in

addition to the capillary force, the van der Waals force between the truncated conical indenter and the substrate also contributes to ant adhesion. The dry interaction can be described by the commonly used Lennard-Jones (L-J) potential,

$$w(r) = 4\varepsilon\left[\left(\frac{\sigma}{r}\right)^{12} - \left(\frac{\sigma}{r}\right)^{6}\right], \tag{13}$$

where ε is a parameter determining the depth of the potential well, σ is a length scale parameter that determines the position of the minimum potential, r is the atom-to-atom distance [23,24]. The total interaction $W(D)$ between the truncated tip and the flat substrate can be obtained by integrals over the volume of the tip and the semi-infinite substrate. Then, the corresponding interaction force can be achieved by the differential of $W(D)$.

Considering the filled liquid at the interface [25], the interaction potential should be integrated separately over parts with different media in the gap. The corresponding Hamaker constants for the interlayer of vacuum (or gas) and liquid are defined, respectively, as

$$A_H^g = 4\pi^2\rho_1\rho_2\varepsilon_g\sigma_g^6, \quad A_H^l = 4\pi^2\rho_1\rho_2\varepsilon_l\sigma_l^6, \tag{14}$$

where ρ_1, ρ_2 are number densities of atoms of the two bodies, respectively; ε_g, σ_g, ε_l and σ_l are parameters in L-J potential corresponding to vacuum (or gas) and liquid medium, respectively.

The van der Waals force between the two solids in the case (a) can be derived as

$$\begin{aligned} F_{vdw}(D) = {} & A_H^l\left[-\frac{1}{6}\cdot\frac{D-R_s}{D^2} + \frac{D_{l0}^6}{168}\cdot\frac{D-7R_s}{D^8}\right] + A_H^g\left[\frac{1}{6}\cdot\frac{D+2h-R_s}{(D+h)^2} - \frac{D_{g0}^6}{168}\cdot\frac{D+8h-7R_s}{(D+h)^8}\right] \\ & + \frac{A_H^l - A_H^g}{6}\cdot\frac{D+R_s-2\sqrt{R_s^2-b^2}}{\left(D+R_s-\sqrt{R_s^2-b^2}\right)^2} - \frac{A_H^l D_{l0}^6 - A_H^g D_{g0}^6}{168}\cdot\frac{D+R_s-8\sqrt{R_s^2-b^2}}{\left(D+R_s-\sqrt{R_s^2-b^2}\right)^8} \\ & + \frac{A_H^g\tan\alpha}{24}\left[4\frac{2R-R_c}{(D+h)^2} - D_{g0}^6\frac{8R-R_c}{7(D+h)^8}\right], \end{aligned} \tag{15}$$

where $R_c = R - (D+h)\tan\alpha$ and the equilibrium distance between the two surfaces across gas or liquid medium is

$$D_{g0} = \left(\frac{2}{15}\right)^{\frac{1}{6}}\sigma_g, \quad D_{l0} = \left(\frac{2}{15}\right)^{\frac{1}{6}}\sigma_l. \tag{16}$$

Equation (15) is also valid for the case (b) with $b = R$.

The van der Waals force in the case (c) is

$$\begin{aligned} F_{vdw}(D) = {} & \frac{A_H^l D_{l0}^6}{168}\left[\frac{D-7R_s}{D^8} - \frac{D+8h-7R_s}{(D+h)^8}\right] - \frac{A_H^l}{6}\left[\frac{D-R_s}{D^2} - \frac{D+2h-R_s}{(D+h)^2}\right] \\ & + \frac{A_H^l\tan\alpha}{24}\left[4\frac{2R-R_c}{(D+h)^2} - D_{l0}^6\frac{8R-R_c}{7(D+h)^8}\right] \\ & + \frac{\left(A_H^g - A_H^l\right)\tan^3\alpha}{6}\cdot\frac{2b-R_c}{(b-R_c)^2} - \frac{\left(A_H^g D_{g0}^6 - A_H^l D_{l0}^6\right)\tan^9\alpha}{6}\cdot\frac{8b-R_c}{7(b-R_c)^8}. \end{aligned} \tag{17}$$

The total interaction force between a single indenter tip and a flat surface can be obtained by summing the capillary force F_c in Eq. (2) and the van der Waals force F_{vdw} in Eq. (15) or Eq. (17).

Considering the multiple microstructured surface on ant footpads, splitting mechanism can be modeled as shown in Fig. 6d, where R_0 denotes the radius of each small asperity. The area ratio η is defined as

$$\eta = \frac{n\cdot\pi R_0^2}{\pi R^2}, \tag{18}$$

where n is the number of the small asperity.

For each splitted asperity, the volume of liquid is

$$V_0 = \frac{V}{n}. \tag{19}$$

It is assumed that no interaction or coalescence happens between asperities when the surface is pulled apart [26]. The total adhesion force of such a multiple microstructured surface is

$$F_{\text{total}} = nF_0 = n\,(F_{c0} + F_{vdw0}), \tag{20}$$

where F_{c0} and F_{vdw0} are the capillary force and van der Waals one for each asperity, respectively.

One should note that the equal load sharing assumption given by Artz et al. [27] is adopted in the present model. Such an assumption is approximately proper only for cases of small adhesive area and normal pulling load.

5 Comparison between the theoretical prediction and experimental result

All the parameters adopted in the theoretical analysis of the four kinds of ants are given in Table 1, which are obtained from the microscopic images with an assumption of circular contact area of each asperity. The radii R, R_0 and area ratio η can be estimated from the corresponding measured areas A and A_0 of the microscopic images, such as $R = \sqrt{A/\pi}$ and $R_0 = \sqrt{A_0/\pi}$. Being consistent with Federle et al. [15,19], we take both the contact angles θ_1 and θ_2 as 15°, the surface tension γ as 0.030 N/m^2 and the separated distance as $D = 100$ nm with a non-dimensional liquid volume $V/(\eta R^2 D) = 5$. Two Hamaker constants are $A_H^g = 6.5 \times 10^{-20}$ J and $A_H^l = 1 \times 10^{-20}$ J [27]. The equilibrium distance between the micro-tip and substrate is $D_{g0} = D_{l0} = 0.2$ nm [28]. Comparison between the theoretical prediction and the experimental measurement is shown in Fig. 7a for the four kinds of ants, where both results agree with each other in the order of magnitude. The adhesion force of *O. smaragdina* is much higher than that of the other three species, which is due to a relatively large contact area and closely patterned microstructure.

For the micro-patterned ant footpad, the adhesion strength is defined as

$$\sigma = \frac{F_{\text{total}}}{S} = \frac{nF_0}{\pi R^2} = \eta \frac{F_0}{\pi R_0^2} = \eta\sigma_0, \tag{21}$$

where the adhesion strength is found to be proportional to the area ratio η and the adhesion strength of a single asperity σ_0.

Comparison between the adhesion strength predicted by the theoretical model and that measured experimentally is shown in Fig. 7b. The variation trend of adhesion strength predicted theoretically agrees qualitatively with that in experiment, though a difference exists for the exact magnitude. Similar to the measurement, the theoretical prediction shows that *O. smaragdina* possesses the highest adhesion strength among the four kinds of ants, while *C. japonicus* has the smallest one. All these demonstrate the importance of the microstructure on ant footpads, which should influence the adhesion significantly. Different shapes and scales of the microstructure will produce an obvious difference of adhesion force and strength. The deviation between experimental and theoretical predictions may be resulted from several factors: (i) The microstructure on ant footpads is not a regular shape, and the distribution of asperities considered in the theoretical model is not exactly the same as the real one. (ii) Interfacial adhesion is assumed to be perfect in our theoretical model, which is not really true in experiment. (iii) No elastic deformation is considered in our model though the arolium of ants is soft. (iv) The detaching behavior of ant footpads may belong to a peel-off case, while the pull-off behavior is only

Table 1 Approximately geometrical parameters of microstructures on different ant footpads for the theoretical calculation of adhesion force

Species	α	R_s/R	A (μm^2)	R (μm)	R_0 (μm)	η
O. smaragdina	0	10	24900	89	2.8	0.8
P. dives	60°	2	4300	37	0.9	0.3
C. japonicus	0	1	3500	33	0.5	0.1
D. rugosum	0	5	2200	26	2.4	0.8

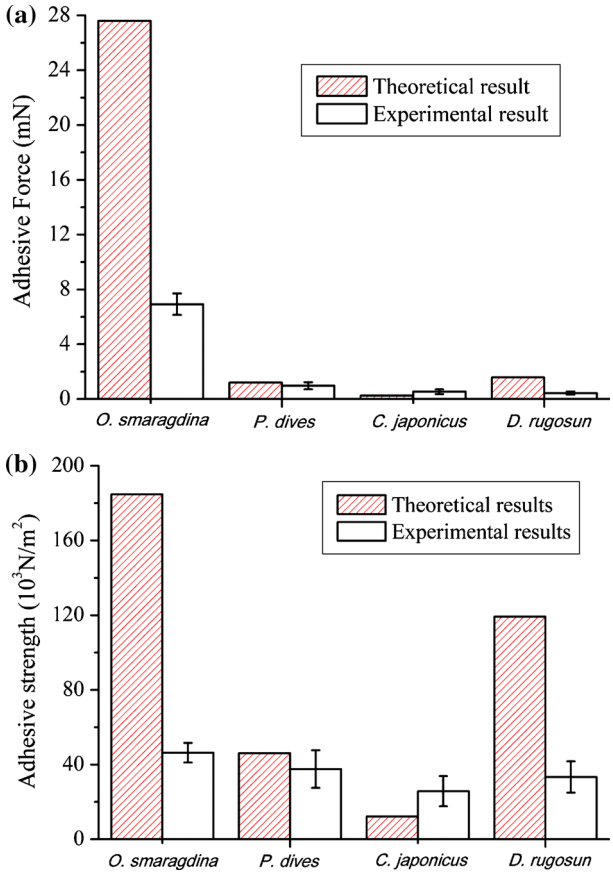

Fig. 7 Comparison of the adhesion force predicted theoretically and experimentally. **a** For the adhesion force of different ant species; **b** for the adhesion strength of different ant species

considered in our theoretical model. Furthermore, the assumption of equal load sharing adopted in the splitting model results in the proportional relation between the adhesion strength and the area ratio as shown in Eq. (21), which may also lead to the deviation of the theoretical predication from the experimental data. A precise peel-off model will be established in the future.

6 Discussion

The effect of several parameters on the interface adhesion is further analyzed. In the theoretical model, the shape of asperities is mainly characterized by two parameters: half of the cone angle α and the non-dimensional radius of curvature of the truncated conical tip R_s/R. The van der Waals force and the capillary one as a function of the separation distance of the indenter tip and the substrate are shown in Fig. 8a, b, where the volume of liquid is assumed to be unchanged. It can be found that the van der Waals force is really a short-range interaction, achieving the maximum at approximately 0.2nm, while the capillary force is a relatively long-range one, extending to a distance of micrometers and significantly influenced by the conical angle at a relatively small separation. The larger the conical angle, the higher the adhesive force is, from which the difference of the adhesive force between *P. dives* and *C. japonicus* can be reasonably explained. Although the configurations of the ended microstructures between *P. dives* and *C. japonicus* are very similar, the conical angle of *P. dives* is larger than that of *C. japonicus*, which results in larger adhesive force. Comparing the van der Waals force and the capillary force further demonstrates that both forces possess the same order of magnitude, which suggests that the van der Waals force may be useful for intimate ant adhesion, especially on an inclined surface to resist the shear sliding.

We further investigate the effect of liquid volume on the capillary force as shown in Fig. 9, where $R_s/R = 4$ and the separation $D = 100\,\text{nm}$. One can see that the liquid volume has a significant effect on the capillary

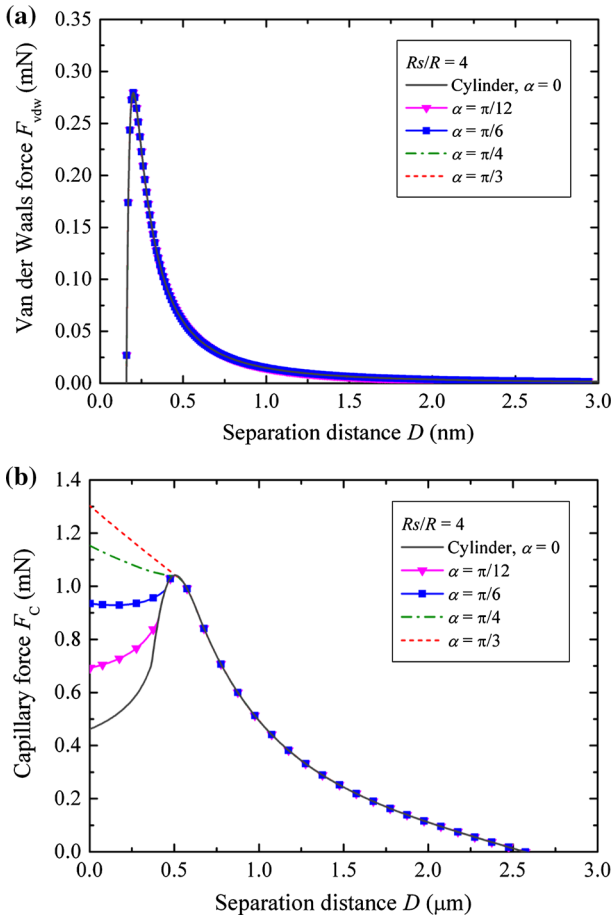

Fig. 8 Adhesion force predicted theoretically as a function of the separation distance for cases with different cone angles but determined parameters $\theta_1 = \theta_2 = 15°$, $\gamma = 0.030\,\mathrm{N/m^2}$, $R = 100\,\mu\mathrm{m}$, $V/R^3 = 0.01$, $n = 1000$, $\eta = 0.5$. **a** The van der Waals force; **b** the capillary force

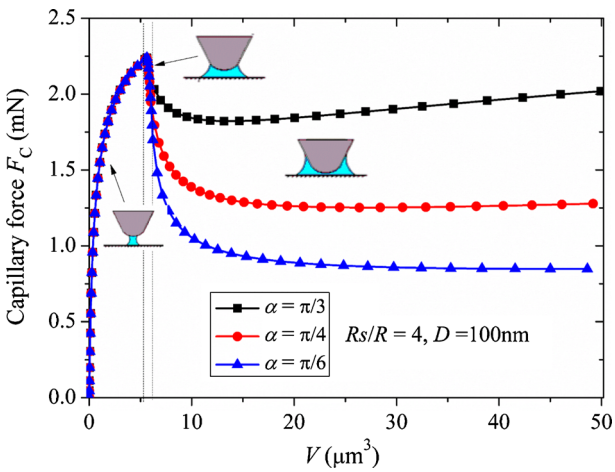

Fig. 9 Effect of liquid volume on the capillary force with a given radius of curvature of spherical tip $R_s/R = 4$ and a fixed separation $D = 100\,\mathrm{nm}$ but with different half of cone angles α

force. When the liquid volume is relatively small at a fixed distance between the tip and the substrate, only part of the truncated conical tip is wetted. In this case, the capillary force increases with the increase in the liquid volume and is insensitive to the cone angle α due to the same radius of curvature of the spherical tip.

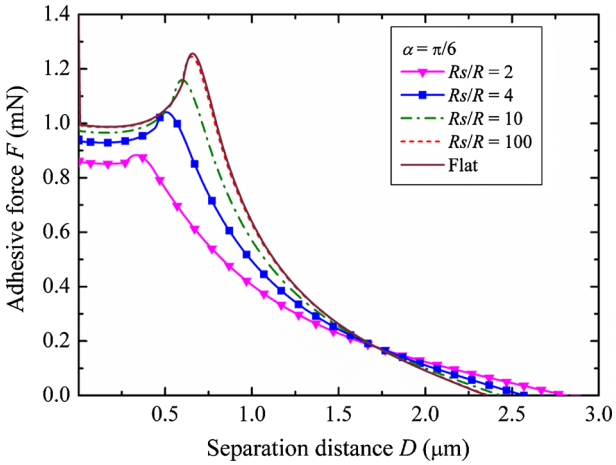

Fig. 10 Adhesion force predicted theoretically as a function of the separation distance for cases with different radii of curvature but determined parameters $\theta_1 = \theta_2 = 15°$, $\gamma = 0.030\,\mathrm{N/m^2}$, $R = 100\,\mu\mathrm{m}$, $V/R^3 = 0.01$, $n = 1000$, $\eta = 0.5$

After the contact line of the meniscus gets to the joint of the conical part and the spherical tip, the capillary force starts to decrease sharply and then increases slightly with an increasing liquid volume. All the results are well consistent with those given in Chen and Soh [20], Qian and Gao [21] and Su et al. [22].

The effect of radius of curvature R_s/R on the force–separation relationship is shown in Fig. 10 with a determined cone angle $\alpha = \pi/6$. Generally, the smaller the curvature of the asperity tip, the larger the adhesion force is. It can be inferred that a cylindrical tip with a small curvature should be an optimized shape for strong capillary force-dominated adhesion. The investigated *O. smaragdina* owns such a kind of footpad, the microstructure of which looks like that on tree frog toe pads [29]. Liquids are secreted from such a footpad to provide capillary force, while channels between patterned surfaces could increase the wetting or de-wetting speed of the contact interface, ensuring the flexibility of the adhesion. Furthermore, liquid can be preserved by channels on each step, so the consumption is reduced. Such a microstructured adhesion pad with channels evolved in nature influences significantly the adhesion force, which may be also useful for the reversible adhesion behavior for this kind of animals. How to realize the reversible adhesion related to capillary force still needs further studies.

Acknowledgments The work reported here was supported by NSFC through Grants #11302228, #11372317, #11532013 and the 973 Nano-project (2012CB937500).

References

1. Beutel, R.G., Gorb, S.N.: Ultrastructure of attachment specializations of hexapods, (Arthropoda): evolutionary patterns inferred from a revised ordinal phylogeny. J. Zool. Syst. Evolut. Res. **39**, 177–207 (2001)
2. Beutel, R.G., Gorb, S.N.: A revised interpretation of the evolution of attachment structures in Hexapoda with special emphasis on Mantophasmatodea. Arthropod Syst. Phylogeny **64**, 3–25 (2006)
3. Stork, N.E.: A scanning electron microscope study of tarsal adhesive setae in the Coleoptera. Zool. J. Linn. Soc. **68**, 173–306 (1980)
4. Autumn, K., Liang, Y.A., Hsieh, S.T., Zesch, W., Chan, W.P., Kenny, T.W., Fearing, R., Full, R.J.: Adhesive force of a single gecko foot-hair. Nature **405**, 681–685 (2000)
5. Niederegger, S., Gorb, S.N.: Friction and adhesion in the tarsal and metatarsal scopulae of spiders. J. Comp. Physiol. A Neuroethol. Sens. Neural Behav. Physiol. **192**, 1223–1232 (2006)
6. Autumn, K., Sitti, M., Liang, Y.C.A., Peattie, A.M., Hansen, W.R., Sponberg, S., Kenny, T.W., Fearing, R., Israelachvili, J.N., Full, R.J.: Evidence for van der Waals adhesion in gecko setae. Proc. Natl. Acad. Sci. USA **99**, 12252–12256 (2002)
7. Gorb, S.N., Beutel, R.G., Gorb, E.V., Jiao, Y.K., Kastner, V., Niederegger, S., Popov, V.L., Scherge, M., Schwarz, U., Votsch, W.: Structural design and biomechanics of friction-based releasable attachment devices in insects. Integr. Comp. Biol. **42**, 1127–1139 (2002)
8. Federle, W., Barnes, W.J.P., Baumgartner, W., Drechsler, P., Smith, J.M.: Wet but not slippery: boundary friction in tree frog adhesive toe pads. J. R. Soc. Interface **3**, 689–697 (2006)
9. Gorb, S., Jiao, Y.K., Scherge, M.: Ultrastructural architecture and mechanical properties of attachment pads in *Tettigonia viridissima* (Orthoptera Tettigoniidae). J. Comp. Physiol. A Neuroethol. Sens. Neural Behav. Physiol. **186**, 821–831 (2000)

10. Gorb, S., Scherge, M.: Biological microtribology: anisotropy in frictional forces of orthopteran attachment pads reflects the ultrastructure of a highly deformable material. Proc. R. Soc. Lond. Ser. B Biol. Sci. **267**, 1239–1244 (2000)
11. Peressadko, A., Gorb, S.N.: When less is more: experimental evidence for tenacity enhancement by division of contact area. J. Adhes. **80**, 247–261 (2004)
12. Chung, J.Y., Chaudhury, M.K.: Roles of discontinuities in bio-inspired adhesive pads. J. R. Soc. Interface R. Soc. **2**, 55–61 (2005)
13. Arzt, E., Gorb, S., Spolenak, R.: From micro to nano contacts in biological attachment devices. Proc. Natl. Acad. Sci. USA **100**, 10603–10606 (2003)
14. Peng, Z.L., Wang, C., Chen, S.H.: Effects of surface wettability on gecko adhesion underwater. Colloids Surf. B Biointerface **122**, 662–668 (2014)
15. Federle, W., Riehle, M., Curtis, A.S.G., Full, R.J.: An integrative study of insect adhesion: mechanics and wet adhesion of pretarsal pads in ants. Integr. Comp. Biol. **42**, 1100–1106 (2002)
16. Federle, W., Brainerd, E.L., McMahon, T.A., Holldobler, B.: Biomechanics of the movable pretarsal adhesive organ in ants and bees. Proc. Natl. Acad. Sci. USA **98**, 6215–6220 (2001)
17. Federle, W., Maschwitz, U., Fiala, B., Riederer, M., Holldobler, B.: Slippery ant-plants and skilful climbers: selection and protection of specific ant partners by epicuticular wax blooms in Macaranga (Euphorbiaceae). Oecologia **112**, 217–224 (1997)
18. Federle, W., Rohrseitz, K., Holldobler, B.: Attachment forces of ants measured with a centrifuge: better 'wax-runners' have a poorer attachment to a smooth surface. J. Exp. Biol. **203**, 505–512 (2000)
19. Federle, W., Baumgartner, W., Holldobler, B.: Biomechanics of ant adhesive pads: frictional forces are rate- and temperature-dependent. J. Exp. Biol. **207**, 67–74 (2004)
20. Chen, S.H., Soh, A.K.: The capillary force in micro- and nano-indentation with different indenter shapes. Int. J. Solids Struct. **45**, 3122–3137 (2008)
21. Qian, J., Gao, H.J.: Scaling effects of wet adhesion in biological attachment systems. Acta Biomater. **2**, 51–58 (2006)
22. Su, Y.W., Ji, B.H., Huang, Y.G., Hwang, K.H.: Effects of contact shape on biological wet adhesion. J. Mater. Sci. **42**, 8885–8893 (2007)
23. Yu, N., Polycarpou, A.A.: Adhesive contact based on the Lennard-Jones potential: a correction to the value of the equilibrium distance as used in the potential. J. Colloid Interface Sci. **278**, 428–435 (2004)
24. Peng, Z.L., Chen, S.H.: Effects of surface roughness and film thickness on the adhesion of a bioinspired nanofilm. Phys. Rev. E **83**, 051915 (2011)
25. Farshchi-Tabrizi, M., Kappl, M., Cheng, Y.J., Gutmann, J., Butt, H.J.: On the adhesion between fine particles and nanocontacts: an atomic force microscope study. Langmuir **22**, 2171–2184 (2006)
26. De Souza, E.J., Brinkmann, M., Mohrdieck, C., Arzt, E.: Enhancement of capillary forces by multiple liquid bridges. Langmuir **24**, 8813–8820 (2008)
27. Arzt, E., Gorb, S., Spolenak, R.: From micro to nano contacts in biological attachment devices. Proc. Natl. Acad. Sci. USA **100**, 10603–10606 (2003)
28. Israelachvili, J.N.: Intermolecular and Surface Forces. Academic Press, London (1992)
29. Persson, B.N.J.: Wet adhesion with application to tree frog adhesive toe pads and tires. J. Phys. Condens. Matter **19**, 376110 (2007)